RSC Advances

PAPER

View Article Online
View Journal | View Issue

Cite this: *RSC Adv.*, 2017, **7**, 16423

MnO_2 *in situ* formed into the pores of C-dots/ZIF-8 hybrid nanocomposites as an effective quencher for fluorescence sensing ascorbic acid†

Guangming Li,[ab] Nan Lv,[ab] Jilin Zhang*[a] and Jiazuan Ni[a]

Received 9th January 2017
Accepted 28th February 2017

DOI: 10.1039/c7ra00307b

rsc.li/rsc-advances

A sensitive fluorescent nanosensor based on MnO_2 quenching fluorescent carbon quantum dots was facilely developed by MnO_2 *in situ* formed in the pores of C-dots/ZIF-8 hybrid nanocomposite. The C-dots/ZIF-8 hybrid nanocomposite was synthesized *via* a rapid method within 5 min at room temperature. Then, the MnO_2 was directly incorporated into the ZIF-8 framework *via* redox reaction between the C-dots/ZIF-8 hybrid nanocomposite and $KMnO_4$. The resulting fluorescent nanosensor exhibited a relatively uniform particle size of about 100 nm, good water-dispersibility and a highly selective fluorescence response toward ascorbic acid with a detection limit as low as 83 nM and a linear range of 0.5–8 μM.

Introduction

Zeolitic imidazolate frameworks (ZIFs) are a subclass of metal–organic frameworks consisting of tetrahedral transition metal ions (zinc/cobalt) bridged by imidazole or imidazolate type linkers. As one of the most promising MOFs, ZIF-8 has received great attention because of its large surface area, unique pore volume, easy preparation, and good water dispersibility.[1,2] When scaled down to the nanoscale level, it can give rise to novel applications in fluorescent probes, delivery vehicles, and therapeutic agents.[3] For example, the fluorescent probe of copper ions has been synthesized by encapsulating BPEI functionalized photoluminescence (PL) carbon dots (C-dots) into the ZIF-8 MOFs.[4] Research results indicated that the accumulation effect of ZIF-8 MOFs can greatly amplify the sensing signal from the C-dots. However, the process of encapsulation is time-consuming (*e.g.* 24 h),[4] and it thus needs to be improved. To date, the hybrid nanocomposites based on ZIF-8 MOFs have shown remarkable properties depending on the incorporated foreign nanoparticles with versatile functions. In most cases, an *in situ* ZIF-8 crystal growth route for construction of the hybrid nanocomposites was applied using foreign nanoparticles as a template.[5–9] However, such hybrid nanocomposites constructed using ZIF-8 as a matrix and the foreign nanoparticles *in situ* formed in the pores of the ZIF-8 are rarely reported, which may be more suitable for those foreign nanoparticles whose morphology and stability cannot be easily controlled.

Recently, manganese dioxide (MnO_2) has been demonstrated to be particularly attractive for bio-applications due to their wide absorption band, redox activity, and good biocompatibility.[10,11] By taking advantage of their broad absorption spectrum (250–550 nm), which overlaps with the fluorescence excitation and/or emission spectra of most types of fluorescent dyes, MnO_2 has been widely studied as a rational quencher for fluorescent sensing systems.[12–14] However, due to the strong tendency of manganese oxide to precipitate or coagulate during the synthesis, most MnO_2 materials for sensing application have larger size and poor water-dispersibility.[12,15–17] In addition, MnO_2, as a surface modification material, introduced in the fluorescence sensing systems, often results in agglomeration of fluorescent nanoparticles.[18–20] Hence, a MnO_2-assistant fluorescent sensor with smaller size and good water-dispersibility for fluorescence sensing is an urgent need.

Ascorbic acid (AA) is an essential nutrient for humans and certain other animals. Ascorbate is a powerful reducing agent, which is capable of rapidly scavenging a number of reactive oxygen species by electron transfer at typical biological pH values. It is well known that the radicals such as the hydroxyl radical are damaging to humans and animals at the molecular level due to their possible interaction with nucleic acids, proteins, and lipids.[21] Certainly, it is very necessary to monitor and determine the content of AA in food and pharmaceutical products to ensure adequate intake using a sensitive fluorescent nanosensor.[22]

In this study, we developed a rapid method for preparing C-dots/ZIF-8 hybrid materials within 5 min and achieved the construction of the C-dots/ZIF-8/MnO_2 *via in situ* formation of MnO_2 using ZIF-8 as a matrix. Due to the broad absorption of MnO_2, it can act as an effective energy quencher adaptable to fluorescent C-dots. When AA was introduced into the

[a]State Key Laboratory of Rare Earth Resource Utilization, Changchun Institute of Applied Chemistry, Changchun 130022, P. R. China. E-mail: zjl@ciac.ac.cn
[b]University of Science and Technology of China, Hefei 244100, P. R. China

† Electronic supplementary information (ESI) available. See DOI: 10.1039/c7ra00307b

nanosensor, the quenched fluorescence could be restored *via* reduction of the quencher MnO_2 to Mn^{2+} by AA. Based on this mechanism, we designed and synthesized the novel C-dots/ZIF-8/MnO_2 hybrid nanocomposite as a selective and sensitive nanosensor for AA fluorescence sensing.

Experimental

Materials

Bovine serum albumin was purchased from Aladdin Industrial Corporation. Ethylenediamine was purchased from Beijing Yili Fine Chemical Co. Ltd. Ascorbic acid was procured from Shanghai Huishi Biochemical Reagents Co., Ltd. Reagent grade NaCl, KCl, $Ca(NO_3)_2$, sodium citrate, glucose and sodium glutamate, were obtained from Beijing Chemical Works. Glutathione and cysteine were purchased from Aladdin Industrial Corporation. Soluble starch and DL-tartaric acid were obtained from Guangdong Xilong Co., Ltd. Vitamin C soluble tablet with 0.1 g of AA content was obtained from Cisen Pharmaceutical Co., Ltd.

Characterization

Powder X-ray diffraction (XRD) patterns were collected on a Bruker D8-FOCUS X-ray diffractometer using Cu Kα radiation. Fourier transform infrared (FTIR) spectra of the samples were recorded on a BRUKER Vertex 70 FTIR spectrometer using a standard KBr pellet technique. Fluorescence measurements were carried out using a Hitachi F-7000 spectrofluorometer. The transmission electron microscopy (TEM) and high-resolution TEM (HRTEM) images were taken with a FEI Tecnai G^2 S-Twin transmission electron microscope operated at 200 kV. Scanning electron microscopy (SEM) images and energy dispersive X-ray spectrum (EDS) were acquired on a field emission scanning electron microscope (FESEM, S4800, Hitachi). Nitrogen-adsorption isotherms were measured at a liquid nitrogen temperature (77 K) using a Micromeritics ASAP 2010M apparatus.

Preparation of the C-dots

The C-dots were synthesized according to the literature[25] with slight modification. In a typical synthesis procedure, citric acid (1.05 g) and ethylenediamine (670 μL) were dissolved in DI-water (10 mL). Then, the solution was transferred to a poly(-tetrafluoroethylene) (Teflon)-lined autoclave and heated at 200 °C for 5 h. After the reaction, the reactors were cooled to room temperature naturally. The product was purified by dialysis (500 Da, MWCO) for approximately 12 h to obtain high quality C-dots. Finally, the C-dots were diluted into 50 mL using DI-water water for further use.

Preparation of C-dots/ZIF-8

First, 1.17 g $Zn(NO_3)_2 \cdot 6H_2O$ was dissolved in 8 mL of the abovementioned C-dots solution. Second, 22.70 g 2-methylimidazole was dissolved in another 80 mL of DI water. The 2-methylimidazole solution was then poured into the mixture of zinc nitrate and C-dots solution with stirring. After stirring for 5 min, the product was collected by centrifugation and then washed with DI water several times. Finally, the C-dots/ZIF-8 nanoparticles were diluted into 10 mL DI water for further use. All the operations were performed at room temperature.

The C-dots/ZIF-8 quenched by various amounts of $KMnO_4$

100 μL of the abovementioned C-dots/ZIF-8 solution was mixed with different amounts of $KMnO_4$ solution, and the purple-red colour of $KMnO_4$ was faded. Subsequently, the mixtures were diluted to 5 mL with 0.05 M Tris–HCl buffer solution (pH = 7.4), followed by shaking and mixing. The fluorescence intensities of different mixtures were collected after another 12 h. All experiments were performed at room temperature. The excitation and emission slits were both 5.0 nm.

Detection of the AA concentrations

For AA fluorescent sensing, the fluorescence probe based on C-dots/ZIF-8/MnO_2 nanocomposite was first prepared. 15 mL $KMnO_4$ solution (5×10^{-4} mol L^{-1}) was slowly added into 5 mL of the abovementioned C-dots/ZIF-8 solution with stirring at room temperature. After continuous stirring for 12 h, C-dots/ZIF-8/MnO_2 nanocomposite was obtained and directly diluted into 25 mL using DI-water. Then, 500 μL of as-obtained C-dots/ZIF-8/MnO_2 solution was diluted to 5 mL with 0.05 M Tris–HCl buffer solution (pH = 7.4) (termed as blank). The fluorescence intensity at 443 nm of the blank sample under excitation with light of 360 nm was measured and marked as F_0. After that, the AA solution with different concentration was added to the abovementioned solution and mixed well. The fluorescence intensities (F) of the samples were measured under the same conditions. The selectivity for AA was confirmed by adding commonly coexisting substances (*i.e.* Na^+, K^+, Ca^{2+}, sodium citrate, glucose, sodium glutamate, glutathione, cysteine, soluble starch, DL-tartaric acid, BSA) instead of AA in a similar way. All detection experiments were performed at room temperature. The excitation slit and the emission slit were both 5.0 nm.

Real sample analysis

For real sample analysis, the AA content of vitamin C soluble tablet (CISEN) was evaluated using C-dots/ZIF-8/MnO_2 hybrid nanocomposite as the nanosensor. Briefly, a tablet (160 mg) with 0.1 g AA content was used to prepare an appropriate concentration of the solution upon analysis using the fluorescence sensing system developed in this study.

Results and discussion

Synthesis and characterization of the C-dots/ZIF-8/MnO_2

Scheme 1 illustrates our design rationale. Carbon dots were chosen due to their outstanding optical properties (*e.g.* resistance to photobleaching), low toxicity, dispersibility in water, excellent biocompatibility and low cost.[23,24] The C-dots were first produced according to a literature method.[25] The as-prepared C-dots have an average particle size of about 4 nm and show an optimum excitation wavelength at 360 nm (ESI, Fig. S1†). The

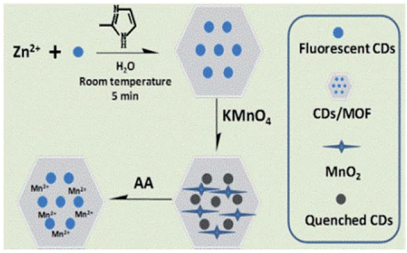

Scheme 1 Schematic of the synthetic route of the C-dots/ZIF-8/MnO_2 and the AA detection process.

carboxylic and N-containing groups of C-dots were confirmed by FTIR analysis, which may play important roles for the formation of C-dots/ZIF-8 *via* the coordination interactions between Zn^{2+} ions (ESI, Fig. S2†).[26] Subsequently, the C-dots/ZIF-8 was prepared by mixing 2-methylimidazole and the mixture of C-dots and $Zn(NO_3)_2 \cdot 6H_2O$ at room temperature using H_2O as solvent with stirring for 5 min. The as-prepared C-dots/ZIF-8 hybrid nanocomposites were spherical and had an average size of about 100 nm (Fig. 1a). The morphology and size did not show significant differences on comparing with the pure ZIF-8 prepared under the same conditions, except for replacing the C-dots solution into water (ESI, Fig. S3†). In addition, the consistency in the XRD pattern between the C-dots/ZIF-8 and simulated ZIF-8 indicates that the introduction of C-dots did not have notable effects on the resulting crystal structure of ZIF-8 (Fig. 1b). Although C-dots could not be directly observed from the TEM image, the same fluorescence emission spectrum and the decrease in specific surface area (from 1091 to 977 $m^2\ g^{-1}$) of C-dots/ZIF-8 can be used as an indirect proof of the encapsulation of nonporous C-dots into the ZIF-8 MOFs (Fig. 1c and d).[7]

The C-dots/ZIF-8/MnO_2 nanocomposite was constructed by incubation of the C-dots/ZIF-8 with the $KMnO_4$. The structure of the product was identified by X-ray diffraction spectroscopy. XRD diffraction peaks of the product prepared by mixing 2-methylimidazole and $KMnO_4$ recorded at 2θ = 11.79, 23.63, 37.01, and 65.57° can be assigned to the (001), (002), (100), and (110) planes of MnO_2 with a turbostratic structure (Fig. 2) based on the literature.[27] Except for the dominant diffraction peaks of the C-dots/ZIF-8, the weak residual peaks of C-dots/ZIF-8/MnO_2 nanocomposite fit well with the MnO_2 phase by comparing with the MnO_2 pattern prepared by mixing 2-methylimidazole and $KMnO_4$ together under the same conditions, which demonstrates that $KMnO_4$ can be reduced to MnO_2 in the presence of C-dots/ZIF-8 for the formation of the stable C-dots/ZIF-8/MnO_2 nanocomposites. In addition, the redox reaction between the C-dots/ZIF-8 nanocomposite and $KMnO_4$ could also be proven by the fading of $KMnO_4$'s purple-red colour. On comparing the FTIR spectrum, the M–O vibration was observed in the C-dots/ZIF-8/MnO_2 nanocomposites in the low frequency region, further indicating that MnO_2 is attached to the C-dots/ZIF-8 sample (ESI, Fig. S4†).[28] The absorption spectrum of the C-dots/ZIF-8/MnO_2 nanocomposite exhibits a wide band in the range of 300–700 nm, which is characteristic absorption of MnO_2 nanoparticles (ESI, Fig. S5†). Moreover, the absorption overlapped well with the fluorescence emission of C-dots.

The application of the C-dots/ZIF-8/MnO_2 for AA detection

Due to the absorption overlapping well with the fluorescence emission of C-dots, MnO_2 could serve as an effective energy acceptor adaptable to fluorescent C-dots.[17] The fluorescence quenching properties of the different concentrations (from 0 to 200 μM) of $KMnO_4$ toward C-dots/ZIF-8 were investigated. As shown in Fig. 3, the fluorescence intensity of C-dots decreased gradually with increasing $KMnO_4$ concentrations. When the $KMnO_4$ concentration was higher than 50 μM, the fluorescence intensity was almost constant, which means that the fluorescence quenching had reached the maximum. Based on the principle of fluorescence detection, too large or too small fluorescence quenching may result in poor sensitivity toward the detection of ascorbic acid. Thus, 30 μM $KMnO_4$ was chosen to synthesize the C-dots/ZIF-8/MnO_2 nanocomposite in this study, which could cause about 85% of the fluorescence quenching.

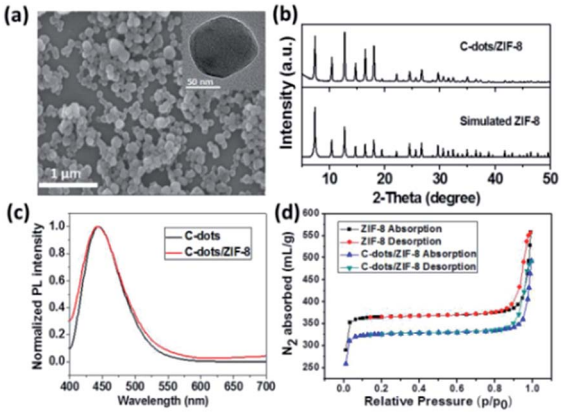

Fig. 1 (a) SEM image of C-dots/ZIF-8 (inset: the corresponding TEM image); (b) XRD patterns of simulated ZIF-8 and C-dots/ZIF-8; (c) normalized photoluminescence emission spectra of C-dots and C-dots/ZIF-8 under the excitation of 360 nm; (d) N_2 sorption isotherms of pure ZIF-8 and C-dots/ZIF-8 collected at 77 K.

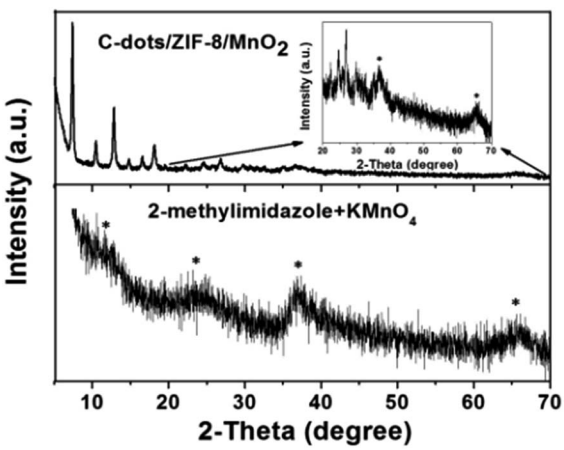

Fig. 2 XRD patterns of CDs/ZIF-8/MnO_2 and MnO_2 prepared by mixing 2-methylimidazole and $KMnO_4$ together.

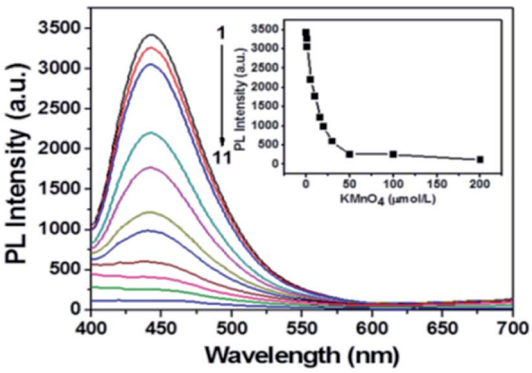

Fig. 3 The C-dots/ZIF-8 quenched by various amounts of $KMnO_4$. Curve 1, C-dots/ZIF-8; curves 2–11, various amounts of $KMnO_4$ were introduced into the C-dots/ZIF-8 solution. Inset, intensity at 443 nm titrated with $KMnO_4$.

The TEM image reveals that the C-dots/ZIF-8/MnO_2 nanocomposites have a smooth surface without MnO_2 deposition, good dispersion and smaller sizes of about 100 nm (Fig. 4a). The Brunauer–Emmett–Teller (BET) isotherm of C-dots/ZIF-8/MnO_2 shown in Fig. 4b exhibits a typical type I isotherm characteristic of microporous materials. The BET surface area of the C-dots/ZIF-8/MnO_2 was ~991 $m^2\ g^{-1}$. Because the manganese content from MnO_2 produced under the optimized conditions was less than the EDS detection limit, the expanded tenfold manganese content of C-dots/ZIF-8/MnO_2 was used to study the distribution of manganese dioxide (ESI, Fig. S6†). The elemental mapping image shows that Mn was distributed in the entire C-dots/ZIF-8 composite, indicating that MnO_2 can be formed within C-dots/ZIF-8 (ESI, Fig. S7†). The possible reason for this is that the permanganate ion was preferentially adsorbed to the inside of the C-dots/ZIF-8 nanocomposite. Subsequently, MnO_2 began to form *via* a redox reaction between the C-dots/ZIF-8 nanocomposite and permanganate ion.

The relationship between the concentration of ascorbic acid and the PL intensity of the C-dots/ZIF-8/MnO_2 nanocomposites was further studied under the optimal conditions. The results show that a significant increase of the PL intensity can be seen with increasing concentrations of AA (Fig. 5a). The recovery efficiency $(F - F_0)/F_0$ displayed a good linear relationship (R =

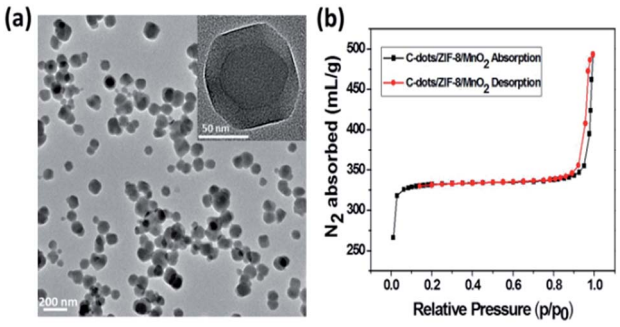

Fig. 4 (a) TEM image of the C-dots/ZIF-8/MnO_2; (b) N_2 sorption isotherms of C-dots/ZIF-8/MnO_2 collected at 77 K.

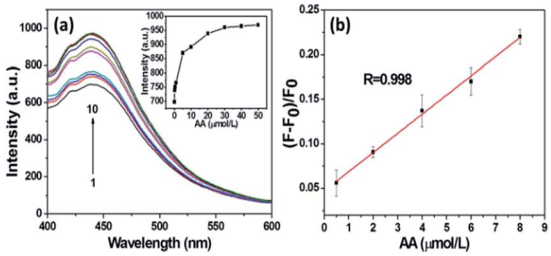

Fig. 5 (a) Fluorescence spectra of the probe in the presence of AA. Curve 1, C-dots/ZIF-8/MnO_2; curves 2–10, various amounts of AA were introduced into the C-dots/ZIF-8/MnO_2 solution (b) the plot of the fluorescence intensity *versus* AA concentration. The error bars represent the standard deviation of three measurements.

0.998) *versus* the concentration of AA in the range of 0.5–8 μM (Fig. 5b), where F_0 and F are PL intensities at 443 nm in the absence and presence of AA, respectively. The limit of ascorbic acid, based on 3σ/slope, was estimated to be about 83 nM.

To assess the selectivity of this novel nanosensor for ascorbic acid, the influence of some electrolytes and biological species was studied in aqueous solutions. The experimental results are presented in Fig. 6. The C-dots/ZIF-8/MnO_2 nanocomposites exhibited a remarkable fluorescence increase toward AA at a concentration of 8 μM. In contrast, relatively weak fluorescence intensity changes could be observed with other molecules even at much higher concentrations. The results showed that the C-dots/ZIF-8/MnO_2 nanocomposites display a highly selective fluorescence response toward AA over other non-target samples. The feasibility of our assay based C-dots/ZIF-8/MnO_2 nanocomposites for fluorescence sensing AA in a real sample was tested. The sample selected was a vitamin C soluble tablet of the CISEN brand, which is commercially available to the public. The composition of each tablet includes 100 mg of AA. The results are summarised in Table S1 in the ESI.† The average

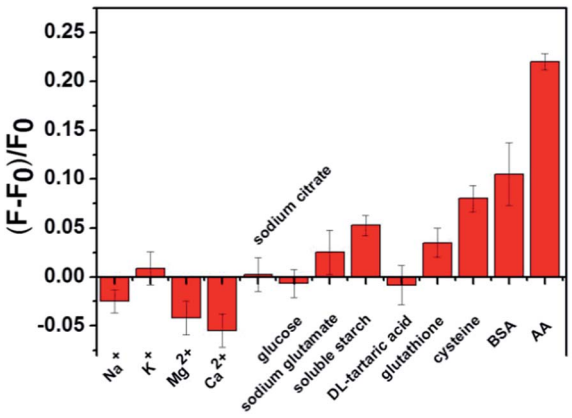

Fig. 6 Selectivity of the probe for AA over other potential interferences (Na^+: 1 mM; K^+: 0.5 mM; Mg^{2+} and Ca^{2+}: 0.25 mM; sodium citrate and glucose: 0.05 mM; sodium glutamate: 0.1 mM; soluble starch, DL-tartaric acid, glutathione, cysteine and bovine serum albumin: 10 μM; AA: 8 μM). F_0 and F are the fluorescence intensity of the probe in the absence and presence of the target (AA) or nontarget samples, respectively.

recovery rate (103.8%) of our system indicates that this fluorescence sensing system based on C-dots/ZIF-8/MnO_2 was likely to be capable of real sample analysis.

Conclusions

In conclusion, we developed a rapid method for preparing C-dots/ZIF-8 hybrid materials within 5 min at room temperature and constructed a C-dots/ZIF-8/MnO_2 probe for sensing ascorbic acid *via* the oxidation–reduction reaction between $KMnO_4$ and C-dots/ZIF-8. Importantly, the C-dots/ZIF-8/MnO_2 nanocomposites with a relatively uniform particle size about 100 nm and good water-dispersibility can serve as an effective probe for PL detection of AA with a detection limit as low as 83 nM, and the linear range is 0.5–8 μM. It is anticipated that the same strategy can also be extended to the preparation of other MnO_2-contained hybrid materials for other applications (*e.g.* photocatalytic and photoelectric studies).

Acknowledgements

This study was supported by the National Natural Science Foundation of China (NNSFC) (Grant No. 21171161 and 21671186).

Notes and references

1 Z. J. Fan, J. Q. Wang, Y. Y. Nie, L. L. Ren, B. Liu and G. Liu, *J. Electrochem. Soc.*, 2015, **163**, B32–B37.
2 Y. C. Pan, Y. Y. Liu, G. F. Zeng, L. Zhao and Z. P. Lai, *Chem. Commun.*, 2011, **47**, 2071–2073.
3 S. X. Li, K. K. Wang, Y. J. Shi, Y. N. Cui, B. L. Chen, B. He, W. B. Dai, H. Zhang, X. Q. Wang, C. L. Zhong, H. N. Wu, Q. Y. Yang and Q. Zhang, *Adv. Funct. Mater.*, 2016, **26**, 2715–2727.
4 X. M. Lin, G. M. Gao, L. Y. Zheng, Y. W. Chi and G. N. Chen, *Anal. Chem.*, 2014, **86**, 1223–1228.
5 W. W. Zhan, Q. Kuang, J. Z. Zhou, X. J. Kong, Z. X. Xie and L. S. Zheng, *J. Am. Chem. Soc.*, 2013, **135**, 1926–1933.
6 X. B. Wang, J. Liu, S. K. Leong, X. C. Lin, J. Wei, B. Kong, Y. F. Xu, Z. X. Low, J. F. Yao and H. T. Wang, *ACS Appl. Mater. Interfaces*, 2016, **8**, 9080–9087.
7 R. Kumar, K. Jayaramulu, T. K. Maji and C. N. Rao, *Chem. Commun.*, 2013, **49**, 4947–4949.
8 Y. H. Song, D. Q. Hu, F. F. Liu, S. H. Chen and L. Wang, *Analyst*, 2015, **140**, 623–629.
9 C. Liu and B. Yan, *RSC Adv.*, 2015, **5**, 101982–101988.
10 C. X. Wang, W. Y. Zhai, Y. X. Wang, P. Yu and L. Q. Mao, *Analyst*, 2015, **140**, 4021–4029.
11 W. W. Zhu, Z. L. Dong, T. T. Fu, J. J. Liu, Q. Chen, Y. G. Li, R. Zhu, L. G. Xu and Z. Liu, *Adv. Funct. Mater.*, 2016, **26**, 5490–5498.
12 C. L. Yang, W. P. Deng, H. Y. Liu, S. G. Ge and M. Yan, *Sens. Actuators, B*, 2015, **216**, 286–292.
13 Q. Y. Cai, J. Li, J. Ge, L. Zhang, Y. L. Hu, Z. H. Li and L. B. Qu, *Biosens. Bioelectron.*, 2015, **72**, 31–36.
14 Y. Xu, X. Chen, R. Chai, C. F. Xing, H. R. Li and X. B. Yin, *Nanoscale*, 2016, **8**, 13414–13421.
15 J. J. Liu, Y. L. Chen, W. F. Wang, J. Feng, M. J. Liang, S. D. Ma and X. G. Chen, *J. Agric. Food Chem.*, 2016, **64**, 371–380.
16 Y. H. Wang, K. Jiang, J. L. Zhu, L. Zhang and H. W. Lin, *Chem. Commun.*, 2015, **51**, 12748–12751.
17 D. G. He, X. X. Yang, X. X. He, K. M. Wang, X. Yang, X. He and Z. Zou, *Chem. Commun.*, 2015, **51**, 14764–14767.
18 R. R. Deng, X. J. Xie, M. Vendrell, Y. T. Chang and X. G. Liu, *J. Am. Chem. Soc.*, 2011, **133**, 20168–20171.
19 J. Yuan, Y. Cen, X. J. Kong, S. Wu, C. L. Liu, R. Q. Yu and X. Chu, *ACS Appl. Mater. Interfaces*, 2015, **7**, 10548–10555.
20 X. D. Wang, D. Wang, Y. L. Guo, C. D. Yang, X. Y. Liu, A. Iqbal, W. S. Liu, W. W. Qin, D. Yan and H. C. Guo, *Biosens. Bioelectron.*, 2016, **77**, 299–305.
21 N. Li, Y. H. Li, Y. Y. Han, W. Pan, T. T. Zhang and B. Tang, *Anal. Chem.*, 2014, **86**, 3924–3930.
22 J. F. Y. Fong, S. F. Chin and S. M. Ng, *Biosens. Bioelectron.*, 2016, **85**, 844–852.
23 D. Li, D. Han, S. N. Qu, L. Liu, P. T. Jing, D. Zhou, W. Y. Ji, X. Y. Wang, T. F. Zhang and D. Z. Shen, *Light: Sci. Appl.*, 2016, **5**, e16120.
24 D. Qu, M. Zheng, J. Li, Z. G. Xie and Z. C. Sun, *Light: Sci. Appl.*, 2015, **4**, e364.
25 S. J. Zhu, Q. N. Meng, L. Wang, J. H. Zhang, Y. B. Song, H. Jin, K. Zhang, H. C. Sun, H. Y. Wang and B. Yang, *Angew. Chem., Int. Ed.*, 2013, **52**, 3953–3957.
26 L. He, T. T. Wang, J. P. An, X. M. Li, L. Y. Zhang, L. Li, G. Z. Li, X. T. Wu, Z. M. Su and C. G. Wang, *CrystEngComm*, 2014, **16**, 3259.
27 H. M. Chen, J. H. He, C. B. Zhang and H. He, *J. Phys. Chem. C*, 2007, **111**, 18033–18038.
28 A. B. Yuan and Q. L. Zhang, *Electrochem. Commun.*, 2006, **8**, 1173–1178.